Rapid Communications

Investigation of contributions of the 2_2^+ resonance in ^{6}He via analysis of the ^{6}He(p, p') reaction

Shoya Ogawa* and Takuma Matsumoto†
Department of Physics, Kyushu University, Fukuoka 819-0395, Japan

(Received 11 March 2020; accepted 13 August 2020; published 27 August 2020)

We investigate the contribution of the 2_2^+ resonance in ^{6}He to observables via analysis of the ^{6}He(p, p') reaction by using the continuum-discretized coupled channels method combined with the complex-scaling method. In this Rapid Communication, we obtain the 2_2^+ state with the resonant energy 2.25 MeV and the decay width 3.75 MeV and analyze contributions of resonances and nonresonant continuum states to the cross section separately. It is found that the 2_2^+ state plays an important role in the energy spectrum. Furthermore, contributions of nonresonant continuum states are also important to clarify the properties of the 2_2^+ state.

DOI: 10.1103/PhysRevC.102.021602

Studies on resonances have attracted much attention in many-body quantum systems for nucleons, quarks, atoms, and so on. In nuclear physics, various resonances have been discovered and investigated their properties, e.g., single-particle resonances, giant resonances, and cluster resonances. Recently, by the development of radioactive ion-beam experiments, resonant structures of nuclei near and beyond the neutron dripline have been intensively pursued. Nuclei on the neutron dripline, such as ^{6}He, ^{11}Li, ^{14}Be, and ^{22}C are known as a two-neutron halo nuclei and have a Borromean structure in which there is no bound state in binary subsystems. To explore resonances of such unstable nuclei, the (p, p') reaction with the inverse kinematics has been often used [1–3], and the contribution of resonances shows up as a peak structure in the excitation energy spectrum observed.

For ^{6}He, low-lying resonances have been discussed by both theoretical and experimental approaches [4–13]. The 2_1^+ state with a small decay width is well understood as the first excited state, and its contribution to cross sections shows up as a sharp peak. The 2_2^+ state, which is considered as the next lower state to 2_1^+, has also been investigated via structural calculations [4–7,9–13] and experimental studies [14,15]. Furthermore, the 2_2^+ state is also considered to play important roles in predicting the properties of some resonant states, e.g., the $3/2_3^-$ state in ^{7}He [10] exists beyond the dripline, and the $3/2_2^+$, $5/2_2^+$ states in the hypernucleus $^7_\Lambda$He [16]. Thus, it is necessary to clear the property of the 2_2^+ state in ^{6}He. However, unfortunately, the contribution of the 2_2^+ state in the energy spectrum does not show a shape structure because its resonant energy is near the right end of the contribution of the 2_1^+ state, and its width is rather large. Thus, the resonant energy (E_r) and the decay width (Γ) of the 2_2^+ state are less clear. To clarify the properties of the 2_2^+ state, it is required an accurate analysis of treating not only resonant contributions, but also nonresonant ones in the energy spectrum.

*s-ogawa@phys.kyushu-u.ac.jp
†matsumoto@phys.kyushu-u.ac.jp

The continuum-discretized coupled-channels (CDCC) method is a reliable method of describing coupling effects to continuum states [17]. At first, CDCC was a method of describing three-body breakup reactions with a two-body projectile, but now it is applicable to analyses of four-body breakup reactions in which a projectile breaks up into three constituents, such as two-neutron halo nuclei [18,19]. In CDCC, an energy spectrum of a breakup cross section is obtained as a continuous function of the excitation energy by using the smoothing procedure based on the complex-scaling method (CSM) [20–23], which is useful for searching resonances in many-body systems. As an advantage of the smoothing procedure, contributions of resonances and nonresonant continuum states in energy spectra are investigated separately. Thus, the CDCC analysis combined with the CSM is indispensable to investigate resonant contributions in energy spectra. Recently, the energy spectrum of the ^{11}Li(p, p') reaction [1] has been analyzed by the approach, and contributions of the resonance and nonresonant continuum states in the energy spectrum have been confirmed [24].

In this Rapid Communication, the 2_2^+ resonant state in ^{6}He is investigated via the CDCC analysis combined with the CSM of ^{6}He(p, p') reactions. In this analysis, the reactions are described as a ^{4}He $+n+n+p$ four-body system, and each resonance in ^{6}He is obtained by the CSM. The calculated elastic and inelastic cross sections are compared with the experimental data, and the effect of the 2_2^+ state on the energy spectrum is discussed by excepting contributions of the 2_1^+ state and nonresonant continuum states.

In the ^{4}He $+n+n+p$ four-body system, the Schrödinger equation based on the multiple scattering is written as

$$\left[K_R + \frac{A_{\rm P}-1}{A_{\rm P}}\sum_{i\in{}^6{\rm He}} g_i + V_C + h - E\right]\Psi(\boldsymbol{\xi}, \boldsymbol{R}) = 0, \quad (1)$$

where $\boldsymbol{R}$ and $\boldsymbol{\xi}$ represent the coordinates between p and the center of mass (c.m.) of ^{6}He and the intrinsic coordinate of ^{6}He, respectively. K_R is a kinetic-energy operator associated with $\boldsymbol{R}$, and h is the internal Hamiltonian of ^{6}He.

As the interaction between nucleons in ^{6}He and p, g_i, the Jeukenne-Lejeune-Mahaux (JLM) effective NN interaction [25] is adopted. Here, it should be noted that we take into account the antisymmetrization between nucleons in ^{6}He and p based on the Kerman-McManus-Thaler (KMT) theory [26,27] as a factor $(A_{\rm P}-1)/A_{\rm P}$ with the mass number $A_{\rm P}$ of ^{6}He . V_C is the Coulomb interaction between the c.m. of ^{6}He and p, that is, Coulomb breakup is neglected in the present analysis.

In CDCC, the scattering wave function with the total spin J and its projection on z-axis M is expanded in terms of a set of eigenstates $\{\Phi^I_n\}$ of ^{6}He as

$$\Psi_{JM}(\boldsymbol{\xi},\boldsymbol{R}) = \sum_{I,n,L} \frac{\chi_\gamma(K_n,R)}{R}\left[\Phi^I_n(\boldsymbol{\xi})\otimes i^L Y_L(\hat{\boldsymbol{R}})\right]_{JM}. \quad (2)$$

Here, I is the internal spin of ^{6}He, and a set of Φ^I_n is generated with the Gaussian expansion method (GEM) [28] in which h is diagonalized by using Gaussian basis functions. As a model space in the present analysis, we take $I^\pi = 0^+$, 1^-, and 2^+ states of ^{6}He. The orbital angular momentum regarding R is L, γ represents $\{n, I, L\}$, and K_n is the relative wave number defined by

$$K_n = \frac{\sqrt{2\mu\left(E-\epsilon^I_n\right)}}{\hbar}, \quad (3)$$

with the reduced mass μ of the ^{6}He -p system and the eigenenergy ϵ^I_n of Φ^I_n. The relative wave-function χ_γ between the c.m. of ^{6}He and p satisfies

$$\left[-\frac{\hbar^2}{2\mu}\frac{d^2}{dR^2}+\frac{\hbar^2L(L+1)}{2\mu R^2}+\frac{A_{\rm P}-1}{A_{\rm P}}U_{\gamma\gamma}(R)+\frac{2e^2}{R}-\left(E-\varepsilon^I_n\right)\right]\chi_\gamma(K_n,R) = -\sum_{\gamma'\neq\gamma}\frac{A_{\rm P}-1}{A_{\rm P}}U_{\gamma\gamma'}(R)\chi_{\gamma'}(K_{n'},R). \quad (4)$$

The coupling potentials $U_{\gamma\gamma'}$ between the γ and the γ' channels are calculated by using the folding model with the JLM interaction in which a normalization factor N_w for the imaginary part is introduced by optimizing the experimental data. Details for the calculation of $U_{\gamma\gamma'}$ are shown in Refs. [24,29].

Solving Eq. (4) under the appropriate boundary condition, we obtain a scattering T matrix represented by T'_{nIL}. Here, it should be noted that T'_{nIL} is not the actual scattering T matrix considered in the present Rapid Communication. In the KMT theory, the actual scattering T matrix T_{nIL} is defined as

$$T_{nIL} = \frac{A_{\rm P}}{A_{\rm P}-1}T'_{nIL}. \quad (5)$$

Details for the KMT theory are shown in Refs. [26,27].

According to the smoothing procedure based on the CSM [23], the double differential cross section (DDX), which depends on the internal energy ε of ^{6}He, and the scattering angle, is described as

$$\frac{d^2\sigma}{d\varepsilon\, d\Omega} = \frac{1}{\pi}{\rm Im}\sum_{iIL}\frac{T^\theta_{iIL}\tilde{T}^\theta_{iIL}}{\varepsilon-\varepsilon^I_{\theta,i}} \quad (6)$$

with

$$\tilde{T}^\theta_{iIL} = \sum_n \left\langle\tilde{\Phi}^I_{\theta,i}\middle|U(\theta)\middle|\Phi^I_n\right\rangle T_{nIL}, \quad (7)$$

$$T^\theta_{iIL} = \sum_n T_{nIL}\left\langle\Phi^I_n\middle|U^{-1}(\theta)\middle|\tilde{\Phi}^I_{\theta,i}\right\rangle. \quad (8)$$

Here, $U(\theta)$ is the scaling transformation operator in the CSM, and $\Phi^I_{\theta,i}$ and $\varepsilon^I_{\theta,i}$ represent the ith eigenstate and energy of ^{6}He, respectively. These states calculated by using the framework combining the GEM and CSM with the scaling angle θ. From Eq. (6), one sees that the DDX is given by an incoherent sum of the contributions of $\Phi_{\theta,i}$. Therefore, we can distinguish between resonant and nonresonant contributions in the DDX.

For the internal Hamiltonian of ^{6}He, we take the Minnesota interaction [30] and the KKNN potential [31] for the n-n and the n-^{4}He interactions, respectively. The particle exchange between valence neutrons and neutrons in ^{4}He is treated with the orthogonality condition model [32]. Furthermore, we introduce the phenomenological three-body potential to reproduce the energies of the ground and 2^+_1 states [33]. As the result, we obtained the ground-state energy -0.972 MeV and $(E_r,\Gamma) = (0.848\ {\rm MeV}, 0.136\ {\rm MeV})$ for the 2^+_1 state.

First, we calculate eigenenergies of ^{6}He by using the CSM with complex-range Gaussian functions [34], which are useful for obtaining resonances with a large decay width. In Fig. 1, the squares represent the eigenenergies of nonresonant continuum states for $I^\pi = 2^+$ with the scaling angle $\theta = 32^\circ$. The circle and triangle describe the eigenenergies of the 2^+_1 and 2^+_2 states, respectively. It is found that the 2^+_2 state has $(E_r,\Gamma) = (2.25\ {\rm MeV}, 3.75\ {\rm MeV})$, and its value is consistent with one calculated by Myo *et al* [10], which provides a better description of the experimental data as mentioned in Ref. [15].

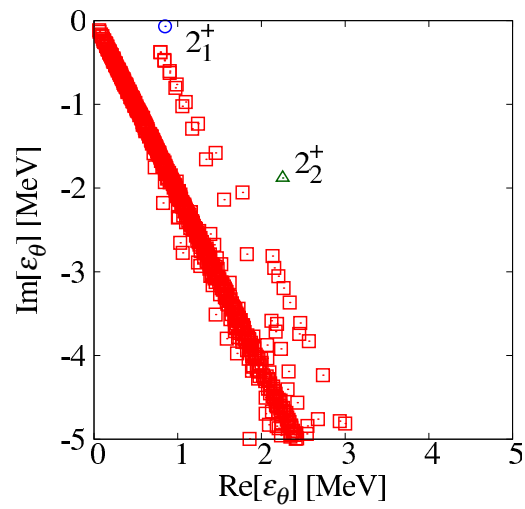

FIG. 1. The eigenvalue distributions for $I^\pi = 2^+$ states in CSM with scaling angle $\theta = 32^\circ$.

TABLE I. Comparing the results of the resonant energy and the decay width (in units of MeV) with those calculated in Ref. [10]. For our calculation, we mention E_r, the excitation energy E_x, and Γ.

	Present results			Ref. [10]	
I^π	E_r	E_x	Γ	E_x	Γ
2_1^+	0.848	1.83	0.136	1.8	0.1
2_2^+	2.25	3.23	3.75	3.5	3.9
0_2^+	3.70	4.68	7.13	4.9	8.8
1_1^-	4.42	5.39	4.82		
1_2^-	4.51	5.48	8.23		

In Table I, all resonances obtained in the present calculation are shown. For the calculation of the DDX, the scaling angle is taken as 32° for the 2_2^+ state and 15° for the other states. In this analysis, the convergence of the calculated DDX has been confirmed.

Next, we calculate angular distributions of the elastic and inelastic cross sections for ^{6}He scattering on p. Figure 2 shows the angular distributions of the elastic cross section at $E/A_P =$ 25, 41, and 71 MeV [2,35–37] in panel (a) and of the inelastic cross section at $E/A_P = 25$ and 41 MeV [2,3] in panel (b).$\theta_{c.m.}$ means the scattering angle in the center-of-mass frame. For the inelastic cross section, the DDX is integrated over ε up to 1.5 MeV, which is the same as the experimental setup at $E/A_P = 41$ MeV [2]. The solid and dashed lines represent the results with the CDCC and those with the so-called one-step calculation, respectively. The one-step calculation neglects multicoupling effects in the CDCC. In the analysis, N_w is taken as 0.8, and it is found that the CDCC well reproduces the experimental data for both elastic and inelastic cross sections simultaneously. The difference between the results of the CDCC and the one-step calculation represents coupling effects. One sees that the effects are particularly important for elastic cross sections at low incident energy and inelastic cross sections.

For the inelastic cross section, we investigate the contribution of the 2_1^+ state. Figure 3 shows the inelastic cross section at $E/A_P = 41$ MeV for each spin-parity state of ^{6}He. The thick solid line is the same as the result of the CDCC in Fig. 2(b). The dotted, dot-dashed, dashed, and thin solid lines denote the contributions for $I^\pi = 0^+$, 1^-, 2^+, and of the 2_1^+ state, respectively. It is found that the contribution for $I^\pi = 2^+$ is dominant and mainly comes from the 2_1^+ state. Furthermore, contributions for $I^\pi = 0^+$ and 1^- are not negligible and come from nonresonant continuum states because resonances for $I^\pi = 0^+$ and 1^- do not exist in $\varepsilon \leqslant 1.5$ MeV. This result shows that the experimental data shown in Fig. 2(b) include not only the contribution of the 2_1^+ state, but also contributions of nonresonant continuum states. In the present calculation, the nonresonant contributions account for about 30% of the total.

Finally, we discuss the contribution of the 2_2^+ state to energy spectra of the breakup cross section in the case of $E/A_P = 41$ MeV. As mentioned above, for the angular distribution of the DDX integrated over ε up to 1.5 MeV, the contribution of the 2_2^+ state is negligible. Therefore, we investigate the angular distribution of the DDX integrated over ϵ from 1.5 to 3 MeV as shown in Fig. 4. The solid line represents the contribution of the 2_2^+ state. The dotted, dot-dashed, and dashed lines describe the contributions for $I^\pi = 0^+$, 1^-, and $I^\pi = 2^+$ without the 2_2^+ state. One sees that the contribution of the 2_2^+ state is more important than the other contributions in $20^\circ \leqslant \theta_{c.m.} \leqslant 30^\circ$. Then, we focus on the energy spectrum around the scattering angle region.

Figure 5(a) shows the energy spectrum for $I^\pi = 2^+$ calculated by integrating the DDX over $\theta_{c.m.}$ from 20° to 30°. The solid line represents the total contribution for $I^\pi = 2^+$. The dotted, dot-dashed, and dashed lines denote the contributions

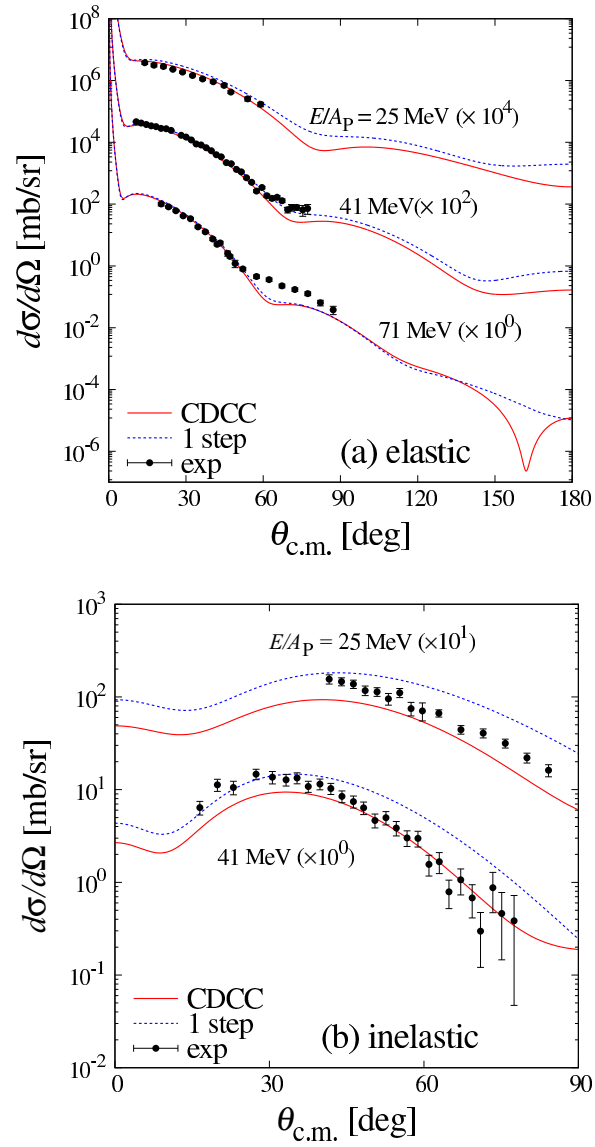

FIG. 2. Angular distributions of the (a) differential elastic cross section at $E/A_P = 25$–71 MeV) and the (b) differential inelastic cross section calculated by integrating the DDX over ε from $\varepsilon = 0$ to 1.5 MeV at $E/A_P = 25$ and 41 MeV. The experimental data are taken from Refs. [2,3,35–37]. Each cross section is multiplied by the factor shown in the figure.

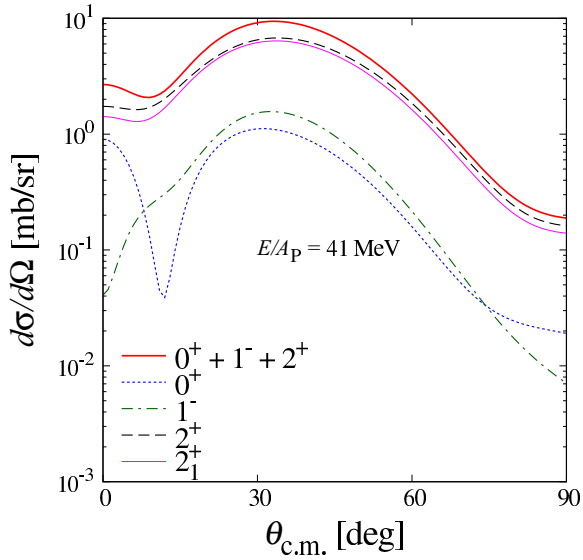

FIG. 3. Angular distributions of the differential cross section calculated by the same way as Fig 2(b) in the case of ^{6}He + p inelastic scattering at $E/A_P = 41$ MeV.

of the 2^+_1, 2^+_2, and nonresonant continuum states, respectively. The strong peak around $\varepsilon = 1$ MeV comes from the 2^+_1 state. Meanwhile, the contribution of the 2^+_2 state shows up as a shoulder peak and is dominant around $\varepsilon = 2$ MeV. Thus, in terms of the cross section for only $I^\pi = 2^+$, the contribution of the 2^+_2 state is rather visible in the energy spectrum.

However, it is difficult to extract a component of a specific spin-parity state from the experimental data. Therefore, we have to confirm how to see the contribution of the 2^+_2 state in the cross section including components from all spin-parity states of ^{6}He. In Fig. 5(b), the solid line represents the energy spectrum with the all components in the present model space, and the dotted line corresponds to the result without the 2^+_2

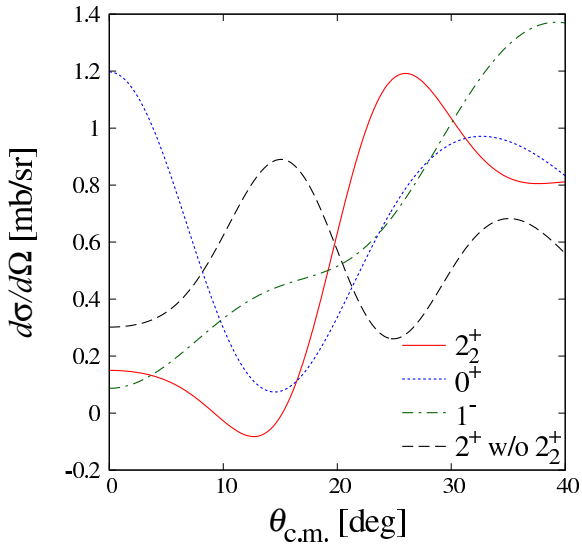

FIG. 4. Angular distributions of the differential cross section calculated by integrating the DDX up from $\varepsilon = 1.5$ to 3 MeV.

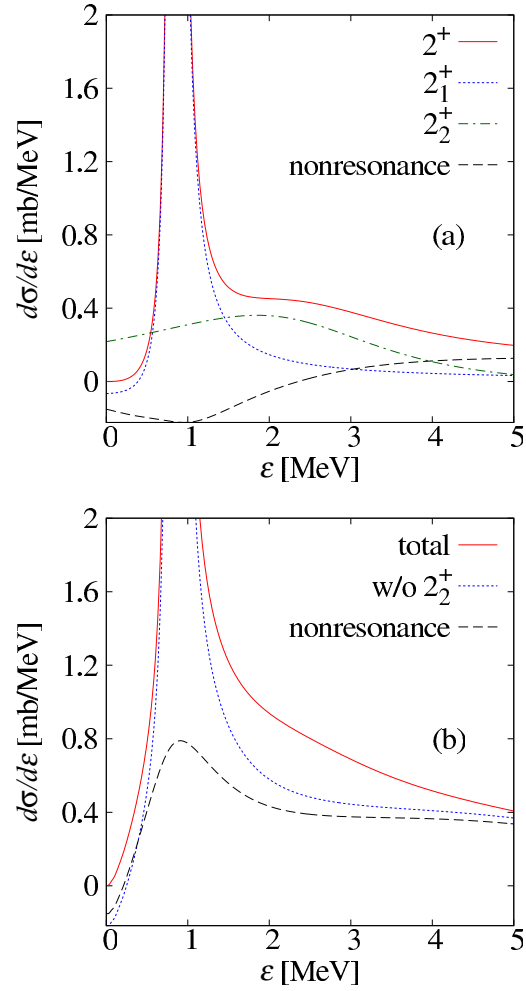

FIG. 5. Energy spectra of the breakup cross section calculated by integrating the DDX up from $\theta_{c.m.} = 20^\circ$ to 30° for $I^\pi = 2^+$ (a) and the sum of all spin-parity states (b).

state. If there was not the 2^+_2 state, the shape of the cross section would be shown by the dotted line. Although a peak structure from the 2^+_2 state does not exist, an increase in the cross section around $\varepsilon = 2$ MeV is found by comparing the solid line with the dotted line. The similar increase in the cross section can be confirmed in the measured energy spectrum from ^{8}He$(p, t)^6$He reaction in Ref. [15]. Therefore, we conclude that the increase in the cross section around $\varepsilon = 2$ MeV indicates the existence of the 2^+_2 state. Here, it should be noted that the low-lying energy spectrum includes contributions of nonresonant continuum states shown by the dotted line. It indicates that one fails to obtain properly the resonant energy and decay width of the 2^+_2 state if the contributions of nonresonant continuum states are neglected.

To clarify the above indication, we fit the breakup cross section up to $\varepsilon = 3$ and 4 MeV by using the Breit-Wigner functions,

$$f(\varepsilon) = \sum_{i=1}^{2} A^i \frac{\Gamma^i/2}{\left(\varepsilon - E^i_r\right)^2 + (\Gamma^i/2)^2}, \tag{9}$$

where A^i, E^i_r, and Γ^i are free parameters, and $i = 1$ and 2 represent the 2^+_1 and 2^+_2 states, respectively. This

TABLE II. Comparing the results of the calculated resonant energy and the decay width (in units of MeV) in the CSM with those obtained by fitting the breakup cross section up to $\varepsilon = 3$ and 4 MeV.

	CSM		Fit (0–3 MeV)		Fit (0–4 MeV)	
I^π	E_r	Γ	E_r	Γ	E_r	Γ
2_1^+	0.848	0.136	0.855	0.144	0.855	0.144
2_2^+	2.25	3.75	1.71	1.97	1.92	2.72

Breit-Wigner parametrization does not take into account effects of nonresonant continuum states. In Table II, the obtained resonant energies and decay widths by fitting are shown. For the 2_1^+ state, E_r and Γ are consistent with the result of the CSM, and nonresonant effects are negligible. Meanwhile, E_r and Γ of the 2_2^+ state are smaller than those calculated in the CSM because nonresonant effects are neglected. Furthermore the properties of the 2_2^+ state, thus, obtained get close to those determined in the ^{8}He$(p,t)^6$He reaction [15]. This implies that the higher resonant energy and broader decay width can be obtained if a detailed analysis taken into account effects of nonresonant continuum states for the ^{8}He$(p,t)^6$He reaction is performed. Therefore, in order to determine the resonant energy and decay width of the 2_2^+ state, an accurate analysis of treating not only resonant contributions, but also nonresonant ones is highly required.

To summarize, we investigated the contribution of the 2_2^+ state in ^{6}He to the breakup cross section via the CDCC analysis combined with the CSM of ^{6}He(p, p') reactions. As the result of the CSM, we obtained the resonant energy and decay width of the 2_2^+ state, which are consistent with those in the previous study. In the analysis of ^{6}He(p, p') reactions, we calculated the angular distributions of the elastic and inelastic scatterings and confirmed importance of coupling effects. For the inelastic cross section, which the DDX is integrated over ε up to 1.5 MeV, it is found that not only the 2_1^+ state, but also nonresonant continuum states contribute substantially to the cross section.

Furthermore, we calculated the breakup cross section by integrating the DDX from $\theta_{\rm c.m.} = 20^\circ$ to 30° to investigate the contribution of the 2_2^+ state to the energy spectrum. As the result, the shoulder peak due to the 2_2^+ state appears in the component for $I^\pi = 2^+$ around $\varepsilon = 2$ MeV, and the effect from the existence of the 2_2^+ state is enhanced in the total components in $\varepsilon = 2$ and 3. Moreover, it is found that the contribution of the nonresonant continuum states to the breakup cross section is also important. Indeed, the nonresonant contribution affects on the resonant energy and decay width estimated from a fitting of cross sections. Thus, an accurate analysis of treating both resonances and nonresonant continuum states is highly required to clarify the properties of the 2_2^+ state. To discuss in more detail, new experimental data are also desired.

This work is supported, in part, by Grant-in-Aid for Scientific Research (Grant No. JP18K03650) from the Japan Society for the Promotion of Science (JSPS).

[1] J. Tanaka *et al.*, Phys. Lett. B **774**, 268 (2017).
[2] A. Lagoyannis *et al.*, Phys. Lett. B **518**, 27 (2001).
[3] S. V. Stepantsov *et al.*, Phys. Lett. B **542**, 35 (2002).
[4] B. V. Danilin, T. Rogde, S. N. Ershov, H. Heiberg-Andersen, J. S. Vaagen, I. J. Thompson, and M. V. Zhukov, Phys. Rev. C **55**, R577 (1997).
[5] S. C. Pieper, R. B. Wiringa, and J. Carlson, Phys. Rev. C **70**, 054325 (2004).
[6] P. Navrátil and W. E. Ormand, Phys. Rev. C **68**, 034305 (2003).
[7] A. Volya and V. Zelevinsky, Phys. Rev. Lett. **94**, 052501 (2005).
[8] N. Michel, W. Nazarewicz, and M. Ploszajczak, Phys. Rev. C **82**, 044315 (2010).
[9] G. Hagen, M. Hjorth-Jensen, and J. S. Vaagen, Phys. Rev. C **71**, 044314 (2005).
[10] T. Myo, K. Katō, and K. Ikeda, Phys. Rev. C **76**, 054309 (2007).
[11] S. Aoyama *et al.*, Prog. Theor. Phys. **94**, 343 (1995).
[12] L. Fortunato, R. Chatterjee, J. Singh, and A. Vitturi, Phys. Rev. C **90**, 064301 (2014).
[13] J. Singh *et al.*, Eur. Phys. J. A **52**, 209 (2016).
[14] J. Jänecke *et al.*, Phys. Rev. C **54**, 1070 (1996).
[15] X. Mougeot *et al.*, Phys. Lett. B **718**, 441 (2012).
[16] E. Hiyama, M. Isaka, M. Kamimura, T. Myo, and T. Motoba, Phys. Rev. C **91**, 054316 (2015).
[17] M. Yahiro *et al.*, Prog. Theor. Exp. Phys. **2012**, 01A206 (2012).
[18] T. Matsumoto, E. Hiyama, K. Ogata, Y. Iseri, M. Kamimura, S. Chiba, and M. Yahiro, Phys. Rev. C **70**, 061601(R) (2004).
[19] T. Matsumoto, T. Egami, K. Ogata, Y. Iseri, M. Kamimura, and M. Yahiro, Phys. Rev. C **73**, 051602(R) (2006).
[20] J. Aguilar and J. M. Combes, Commun. Math. Phys. **22**, 269 (1971).
[21] E. Balslev and J. M. Combes, Commun. Math. Phys. **22**, 280 (1971).
[22] S. Aoyama *et al.*, Prog. Theor. Phys. **116**, 1 (2006).
[23] T. Matsumoto, K. Katō, and M. Yahiro, Phys. Rev. C **82**, 051602(R) (2010).
[24] T. Matsumoto, J. Tanaka, and K. Ogata, Prog. Theor. Exp. Phys. **2019**, 123D02 (2019).
[25] J.-P. Jeukenne, A. Lejeune, and C. Mahaux, Phys. Rev. C **16**, 80 (1977).
[26] A. K. Kerman, H. McManus, and R. M. Thaler, Ann. Phys. (NY) **8**, 551 (1959).
[27] K. Minomo, K. Washiyama, and K. Ogata, arXiv:1712.10121.
[28] E. Hiyama, Y. Kino, and M. Kamimura, Prog. Part. Nucl. Phys **51**, 223 (2003).
[29] T. Matsumoto, D. Ichinkhorloo, Y. Hirabayashi, K. Katō, and S. Chiba, Phys. Rev. C **83**, 064611 (2011).
[30] D. R. Thompson, M. Lemere, and Y. C. Tang, Nucl. Phys. A **286**, 53 (1977).
[31] H. Kanada *et al.*, Prog. Theor. Phys. **61**, 1327 (1979).
[32] S. Saito, Prog. Theor. Phys. **41**, 705 (1969).
[33] F. Ajzenberg-Selove, Nucl. Phys. A **490**, 1 (1988).
[34] S. Ohtsubo *et al.*, Prog. Theor. Exp. Phys. **2013**, 073D02 (2013).
[35] L. Giot *et al.*, Phys. Rev. C **71**, 064311 (2005).
[36] A. A. Korsheninnikova *et al.*, Nucl. Phys. A **617**, 45 (1997).
[37] T. Uesaka *et al.*, Phys. Rev. C **82**, 021602(R) (2010).